



High Fluid-Pressure Patches Beneath the Décollement: A Potential Source of Slow Earthquakes in the Nankai Trough off Cape Muroto

Hirose, T. ; Hamada, Y. ; Tanikawa, W. ; Kamiya, N. ; Yamamoto, Yuzuru ; Tsuji, T. ; Kinoshita, M. ; Heuer, V. B. ; Inagaki, F. ; Morono, Y. ...

(Citation)

Journal of Geophysical Research: Solid Earth, 126(6):e2021JB021831

(Issue Date)

2021-06-16

(Resource Type)

journal article

(Version)

Version of Record

(Rights)

© 2021. The Authors.

This is an open access article under the terms of the Creative Commons Attribution-NonCommercial-NoDerivs License, which permits use and distribution in any medium, provided the original work is properly cited, the use is non-commercial and no...

(URL)

<https://hdl.handle.net/20.500.14094/0100476476>



JGR Solid Earth

RESEARCH ARTICLE

10.1029/2021JB021831

Key Points:

- A transient borehole mud flow confirmed the existence of an overpressured aquifer beneath the Nankai Trough décollement off Cape Muroto
- The aquifer of ~5–10 MPa excess pore pressure was distributed over a lateral extent of hundreds of meters
- The overpressured aquifer may have been the cause of slow earthquakes observed near the drilling site

Supporting Information:

Supporting Information may be found in the online version of this article.

Correspondence to:

T. Hirose,
hiroset@jamstec.go.jp

Citation:

Hirose, T., Hamada, Y., Tanikawa, W., Kamiya, N., Yamamoto, Y., Tsuji, T., et al. (2021). High fluid-pressure patches beneath the décollement: A potential source of slow earthquakes in the Nankai Trough off Cape Muroto. *Journal of Geophysical Research: Solid Earth*, 126, e2021JB021831. <https://doi.org/10.1029/2021JB021831>












Received 31 JAN 2021

Accepted 27 MAY 2021

© 2021. The Authors.

This is an open access article under the terms of the [Creative Commons Attribution-NonCommercial-NoDerivs License](#), which permits use and distribution in any medium, provided the original work is properly cited, the use is non-commercial and no modifications or adaptations are made.

High Fluid-Pressure Patches Beneath the Décollement: A Potential Source of Slow Earthquakes in the Nankai Trough off Cape Muroto

T. Hirose¹ , Y. Hamada¹ , W. Tanikawa¹ , N. Kamiya² , Y. Yamamoto³ , T. Tsuji⁴ , M. Kinoshita⁵ , V. B. Heuer⁶ , F. Inagaki⁷ , Y. Morono¹ , and Y. Kubo¹ 

¹Kochi Institute for Core Sample Research (X-star), Japan Agency for Marine-Earth Science and Technology (JAMSTEC), Kochi, Japan, ²Graduate School of Engineering, Kyoto University, Kyoto, Japan, ³Department of Planetology, Graduate School of Science, Kobe University, Kobe, Japan, ⁴Department of Earth Resources Engineering, Kyushu University, Fukuoka, Japan, ⁵Earthquake Research Institute, University of Tokyo, Tokyo, Japan, ⁶MARUM-Center for Marine Environmental Sciences, University of Bremen, Bremen, Germany, ⁷Mantle Drilling Promotion Office, Institute for Marine-Earth Exploration and Engineering (MarE3), JAMSTEC, Yokohama, Japan

Abstract Pore pressure plays a key role in the generation of earthquakes in subduction zones. However, quantitative constraints for its determination are quite limited. Here, we estimate the subsurface pore pressure by analyzing the transient upwelling flow of drilling mud from borehole C0023A of the International Ocean Discovery Program (IODP) Expedition 370, in the Nankai Trough off Cape Muroto. This upward flow provided the first direct evidence of an overpressured aquifer in the underthrust sediments off Cape Muroto. To estimate the pre-drilling pore pressure in the overpressured aquifer around a depth of 950–1,050 m below sea floor, we examined the measured porosities of core samples retrieved from nearby IODP wells; we then proceeded to explain the observed time evolution of the flow rate of the upwelling flow by modeling various sized aquifers through solving a radial diffusion equation. It was observed that for a permeability of 10^{-13} m^2 , the aquifer possessed an initial excess pore pressure of ~5–10 MPa above the hydrostatic pressure, with a lateral dimension of several hundred meters and thickness of several tens of meters. The overpressure estimates from the porosity-depth profile at Site C0023 differ from those at other drill sites in the region, suggesting the possible existence of multiple overpressured aquifers with a patchy distribution in the underthrust sediments of the Nankai Trough. As pore pressure is relevant in maintaining fault stability, the overpressured aquifers may be the source of slow earthquakes that have been observed around the drilling site.

Plain Language Summary Fault zones often act as barriers to fluid flow, which can lead to the formation of aquifers of pressurized fluid in the vicinity of the fault. It is well known that pore fluid pressure plays a key role in the generation of subduction zone earthquakes, however quantification of pore fluid pressures around subduction zone faults has, up to now, been limited. The International Ocean Discovery Program (IODP) Expedition 370 drilled the Nankai Trough subduction zone off Cape Muroto (Japan), where slow earthquakes have been observed. While drilling, we observed a transient upwelling flow of drilling mud from the borehole. This flow provided the first direct evidence of an overpressured aquifer around the plate boundary fault. To constrain the properties of the aquifer we modeled aquifers with varying properties, and found that the upwelling mud at the drill-site was likely generated by an aquifer with a lateral extent of hundreds of meters and with pore pressures considerably higher than the typical (hydrostatic) pore fluid pressure expected at this depth. Our results suggest that slow earthquakes that occur near Cape Muroto may be caused by relatively small, scattered, highly-pressurized subsurface aquifers like the one we intersected during Expedition 370.

1. Introduction

Pore fluid pressure plays a key role in the structural development of accretionary complexes (e.g., Davis et al., 1983) and fault movements that cause earthquakes in subduction zones (e.g., Moore & Vrolijk, 1992; Saffer & Tobin, 2011). Slow earthquakes, including tremors, very low-frequency events, and slow slip events, have been detected in subduction zones over the past 20 years (e.g., Obara & Kato, 2016). The generation

and migration of slow earthquakes have been attributed to changes in the strength and stability of faults in response to increases in pore pressure (e.g., Kodaira et al., 2004; Scholz, 1998). Nonetheless, despite the important role of pore pressure in fault mechanics, the magnitude and distribution of pore pressure within subduction zones remains poorly constrained.

Previous studies have investigated pore pressure in sediments beneath shallow plate boundary décollements in several subduction zones (e.g., Nankai, Costa Rica, and Barbados subduction zones). Among them, the Nankai Trough, particularly off Cape Muroto, has been studied intensively. The various investigative techniques used include the inversion of porosities measured in drilled cores (e.g., Screaton et al., 2002), numerical modeling of fluid flow using laboratory-derived permeability and sediment consolidation (e.g., Gamage & Screaton, 2006; Saffer, 2003), generic transformations from seismic velocity to porosity and effective stress (e.g., Tobin & Saffer, 2009) and the use of theoretical crack closure models to estimate pore pressure from seismic velocity (Tsuji et al., 2008). All these studies conclude that pore pressures in sediments at and beneath the décollement zone exceed the hydrostatic pressure (i.e., those sediments are overpressured). However, there remains a lack of direct evidence of high pore pressure in sediments around the plate boundary off Cape Muroto.

The International Ocean Discovery Program (IODP) Expedition 370 recently revisited the Nankai Trough off Cape Muroto (Heuer et al., 2017), where slow earthquakes were characteristically observed (Figure 1). Drilling at Site C0023 during Expedition 370 successfully penetrated the entire sequence of prism, décollement and underthrust sediments. During drilling within the underthrust section, we coincidentally observed an upwelling flow of drilling mud from the borehole. This upwelling flow provided the first direct evidence of overpressured sediments below the décollement zone off Cape Muroto. In this study, we first estimate the expected pore pressure using the porosity-depth profile measured from drilled cores. We then use the drilling data and the observed flow rate to determine the pore pressure in excess of hydrostatic pressure in the underthrust sequence by solving an analytical solution. We also assess the size of the overpressured aquifer that activated the upwelling of drilling mud. Finally, the pore pressures estimated from the porosity data and the numerical modeling at Site C0023 are compared with previously reported values from neighboring sites to discuss the spatial distribution of overpressured aquifers in the shallow parts of the Nankai subduction zone.

2. Geology at Site C0023

The Nankai accretionary complex is formed by the subduction of the Philippine Sea Plate beneath the Eurasian Plate in southwest Japan. The complex has been investigated by seafloor drilling, seismic reflection surveys, and seismic event observations at various locations along the Nankai Trough (Shipboard Scientific Party, 1991, 2001a, 2001b; Tobin & Kinoshita, 2006). Off Cape Muroto in particular, subseafloor drilling by the Ocean Drilling Program has penetrated the entire accretionary prism, including the décollement zone and basalt basement, at several sites within the 3-D seismic reflection volume that extends across the trench (Figure 1). High pore-pressure within the underthrust sediments below the décollement at these sites has been inferred from both depth profiles of porosity, and seismic reflection data (e.g., Screaton et al., 2002; Tsuji et al., 2008).

Expedition 370 drilled at Site C0023 (32°22.0018'N, 134°57.9844'E, 4,776 m water depth), close to Sites 808 and 1174. Heuer et al. (2017) identified four main lithostratigraphic units at Site C0023 (Figure 2a). The near-surface sediments are Quaternary trench-fill facies (TF, seafloor to 494 meters below seafloor, mbsf) of silty and sandy turbidites interbedded with mudstone. The underlying Pliocene to Quaternary Upper Shikoku Basin facies (USB, 494–637 mbsf) consists of hemipelagic mudstone with interbedded tuff. Below facies USB, the mid-Miocene to Pliocene Lower Shikoku Basin facies (LSB, 637–1112 mbsf) is composed of homogeneous volcanoclastics-bearing hemipelagic mudstone with dips of 5°–30°. The acidic volcanoclastic facies (AV, 1112–1126 mbsf) is the deepest sedimentary unit and comprises mudstone and felsic ash overlying basaltic hyaloclastite. At Site C0023, Heuer et al. (2017) identified the décollement as a nearly horizontal zone from 758 to 796 mbsf within LSB facies that is characterized by a dense population of faults/fractures and mineral veins.

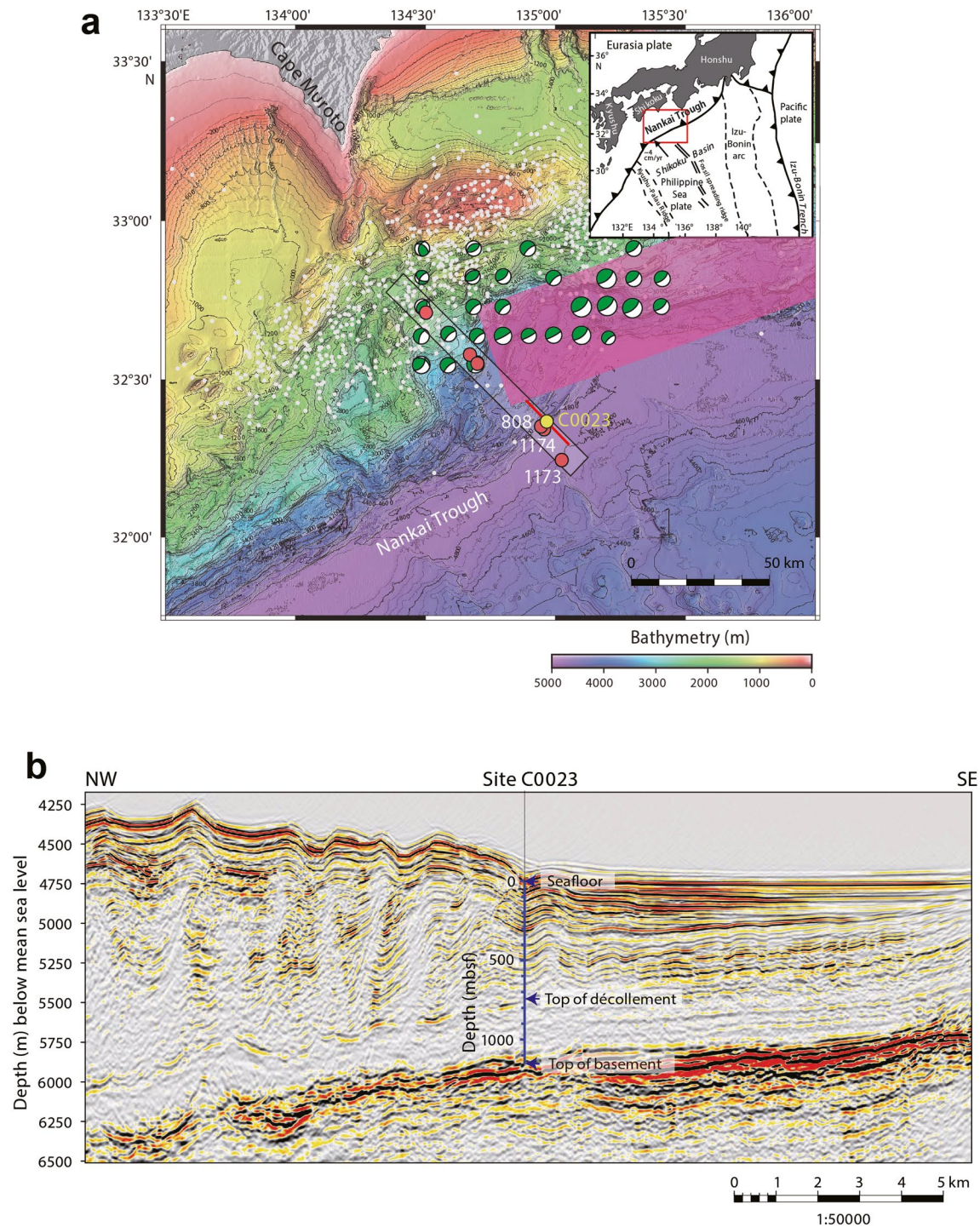


Figure 1. (a) Regional bathymetric map of the area around the drilling site (modified from Heuer et al., 2017) showing locations of Site C0023 (yellow) and nearby Ocean Drilling Program drill sites (red). Black rectangle delineates area of a 3-D seismic survey along the Muroto Transect (Moore et al., 2001). White dots are the epicenter locations of very low frequency earthquakes (VLFs) observed between 2003 and 2018 (Asano et al., 2008; Nakano et al., 2018). Plotted focal mechanisms are the solutions of the largest magnitude VLF between 2003 and 2018 (compiled from Takemura et al., 2019). The pink shaded rectangle is the estimated area of the 2017–2018 slow slip event (Yokota & Ishikawa, 2020). Inset: Simplified plate tectonics of the area southeast of the Japanese Islands. (b) Prestack seismic depth migration section through Site C0023 (shown by the red line in (a)). Vertical blue line shows the trace of drill hole C0023 with depth scale in meters below seafloor (mbsf); the horizons interpreted to represent the seafloor, top of décollement zone and top of oceanic basement, are labeled.

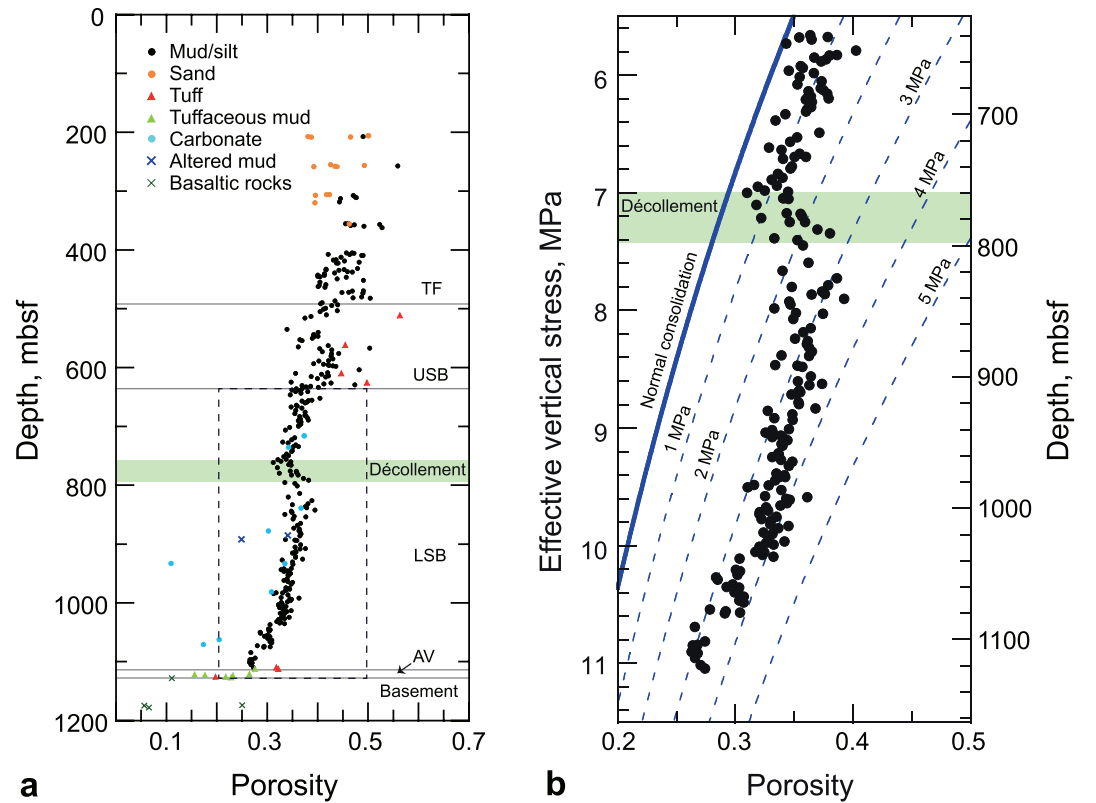


Figure 2. (a) Depth profile of porosity at Site C0023. TF, trench-fill facies; USB, Upper Shikoku Basin; LSB, Lower Shikoku Basin facies; AV, acidic volcanoclastic facies. (b) Porosity profile within LSB facies (area within dashed box in (a)) as a function of effective vertical stress (i.e., difference between lithostatic and hydrostatic pressures). Solid blue line is the porosity versus effective vertical stress relationship defined from reference site (Site 1173) assuming hydrostatic pore pressure (i.e., a normal consolidation curve). Dashed lines are contours of excess pore pressure above the normal consolidation curve.

3. Pore Pressure Estimated From Porosity Profiles

3.1. Previous Estimations of Pore Pressure in the Nankai Trough

Screaton et al. (2002) estimated the pore pressure in LSB facies from the depth trend of porosity data. They focused on the landward trend in porosity along the Muroto transect, from Site 1173 near the outer margin of the trench to Sites 1174 and 808 within the accretionary prism (Figure 1a). They found that the porosity (ϕ) of LSB facies at Site 1173 decreases steadily with depth (Figure S1c), and fits the depth–porosity–compaction relationship defined by Rubey and Hubbert (1959) as

$$\phi = \phi_0 e^{-\beta \sigma'_v}, \quad (1)$$

where ϕ_0 is the reference porosity, β is the bulk compressibility (that includes compressibility of the fluid, the solid grain, and grain rearrangement), and σ'_v is the effective vertical stress, expressed as

$$\sigma'_v = \sigma_v - P_f = \sigma_v - (P_{hy} + \Delta P). \quad (2)$$

σ_v is the vertical stress, P_f is the formation pore pressure, P_{hy} is the hydrostatic pressure, and ΔP is the excess pore pressure above the hydrostatic pressure (i.e., the amount of overpressure). Vertical stress σ_v and hydrostatic pressure P_{hy} can be obtained by integrating the bulk density of sediments and that of seawater, respectively, and are given by

$$\sigma_v(z') = g \int_0^{z'} \rho_s(z') dz' + g \rho_w z_{sf}, \text{ and} \quad (3)$$

$$P_{hy}(z) = g \int_0^z \rho_w(z) dz, \quad (4)$$

where z is the depth from the sea level, z' is the depth below seafloor, z_{sf} is the seafloor depth, ρ_s is the bulk density of the wet sediments measured from core samples, and ρ_w is the density of seawater (1.024 g/cm^3). We used the constant ρ_w , as it only varies by $\pm 2.5\%$ under the pressure and temperature conditions of the drilling interval at Site C0023. If it is assumed that the sediments in LSB facies below the décollement are not overpressured ($\Delta P = 0$ in Equation 2), the porosity trend at Site 1173 fits Equation 1 with $\phi_0 = 0.704 \pm 0.01$ and $\beta = 0.132 \pm 0.004 \text{ Pa}^{-1}$ (Figure S1d).

In contrast, porosities below the décollement at Sites 808 and 1174 (Figure S1a and S1b) are high relative to the depth trend of porosity at Site 1173 (Figure S1c and S1d). Sreaton et al. (2002) attributed the porosity increase below the décollement to overpressured sediments. They estimated the amount of excess pore pressure by comparing the porosity trends of the underthrust sediments at Sites 1174 and 808 with those of the reference site (1173), under the assumption that the volume of solid material in the sediments is constant, and that the porosities at Site 1173 provide a reasonable proxy for the condition of the sediments at Sites 808 and 1174 before they had been subducted beneath the trench. They extended the ϕ – σ'_v relationship that was determined from LSB facies at Site 1173 (Figure S1d) to the depth intervals of LSB facies at Sites 1174 and 808, and then calculated the ΔP values necessary to explain the observed porosities below the décollement at those sites. ΔP was estimated to be 3.6 and 4.2 MPa below the décollement at Sites 1174 and 808, respectively (Sreaton et al., 2002). In this study, we apply the same method as Sreaton et al. (2002) to the porosity data obtained from core samples at Site C0023.

3.2. Porosity Measurement at Site C0023

Porosity of core samples collected at Site C0023 was measured using a helium gas pycnometer onboard the drilling vessel *Chikyu*. About 20 cm^3 of undisturbed sediments was taken from split cores in a weighted glass beaker, and wet sediment mass was measured using a high-precision digital balance system. The sample was then dried in a convection oven for 24 h at 105°C , then brought to room temperature while keeping it in a desiccator for 1 h. Dry sediment mass and volume were measured using the balance system and the pycnometer, respectively. Standard ODP/IODP practices were then used to determine the mass and volume of pore water, salt, and solid grain (Blum, 1997). From these data, porosity was calculated (more details in Heuer et al., 2017). Errors in porosity measurements when using this method can be due to rebound effects when pressure at depth is released, or due to smectite dehydration during oven-drying of sediments. We assume that these errors affected the samples retrieved from three sites (Sites C0023, 808, and 1174) in a similar manner, and therefore, the porosity-depth trends between the different sites should be comparable.

3.3. Porosity Profile and Estimated Pore Pressure at Site C0023

The porosity-depth profile at Site C0023 (Figure 2a) is similar to those at Sites 808 and 1174 (Figure S1). At Site C0023, the porosity in facies TF and USB shows an overall (but highly variable) decreasing trend with depth. Within LSB facies, porosity continues to decrease down to the top of the décollement zone at 760 mbsf, below which it increases gradually by 5%–7% to 830 mbsf. Below 830 mbsf, porosity resumes a general compaction trend through to the base of LSB facies, and then decreases rapidly within facies AV, where tuffaceous mud is the dominant lithology. We focused on the porosity data below the décollement in LSB facies for the estimation of ΔP (shown in Figure 2b) using the method described in Section 3.1. We also considered the porosities at Site 1173 as a reasonable proxy for the condition of the sediments at Site C0023 before they had been subducted beneath the trench.

The trend of porosity for sediments above the décollement zone roughly follows the 1 MPa ΔP contour (Figure 2b). However, with increasing depth below the top of the décollement zone (760 mbsf) to the bottom of the underthrust sediments (1,110 mbsf), the porosity trend shifts to higher values of ΔP . From the top

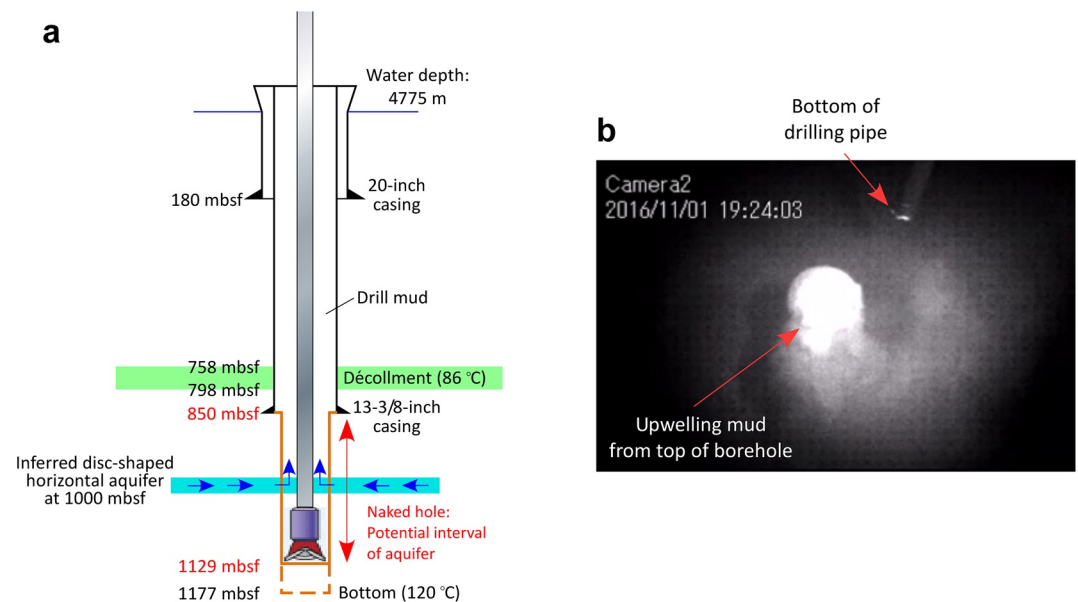


Figure 3. (a) Borehole configuration of Hole C0023 when upwelling flow of drilling mud was observed. For modeling of pore fluid pressure and flow rate, a horizontal disk-shaped aquifer at 1,000 mbsf was assumed. (b) An image of the upwelling mud flow from the well head of Hole C0023 on November 1, 2016 (see also Movie S1).

of the décollement, ΔP increases gradually from around 1.0 MPa at 760 mbsf to 4.2 MPa at 1,020 mbsf, and then decreases to 3.0 MPa at 1,110 mbsf. The highest value of ΔP (4.2 MPa at 1020 mbsf) corresponds to $\lambda^* = 0.42$, where λ^* is the modified pore pressure ratio, defined by Shi and Wang (1988) as the ratio of excess pore pressure to effective lithostatic stress. Our estimates of pressure at Site C0023 are consistent with those reported by Screatton et al. (2002) for Sites 1174 and 808.

4. Excess Pore Pressure Estimated by Analysis of Upwelling Flow of Drilling Mud

4.1. Observations of Upwelling Flow

The observation of an upwelling flow of drilling mud from the open borehole provided an unprecedented opportunity to estimate in situ pore pressure. Thus, ΔP was estimated by analyzing the flow of upwelling drilling mud. To protect the fragile décollement zone (758–796 mbsf), the casing was set to a depth of 850 mbsf. After the full sequence of LSB facies had been penetrated (at 1,129 mbsf; Figure 3a), the drill string was pulled from the borehole. At this time, mud flow from the well-head was confirmed by an underwater TV camera that had been lowered to the seafloor (Figure 3b). The expulsion of drilling mud through the casing pipe provided direct evidence for the existence of a high-pressure aquifer somewhere between 850 and 1,129 mbsf.

We had three opportunities to view the head of the casing at the seafloor via an underwater TV camera. The first was at 19:00 on November 1, 2016, when upwelling of drilling mud from the borehole was noted while pulling the drill bit out of the hole. The flow shown on the TV monitor was recorded with a digital video camera; the flow velocity (v in Equation 6 below) was calculated to be ~ 0.1 m/s by tracing the movement of particles emitted from the casing head on the time-elapsd snapshots of the movie with frame rate of 30 fps (Movie S1). The second observation was at 18:30 on November 4, 2016. Mud was still flowing out from the well head, but the flow was clearly weaker than on November 1. No video recording of this was made, so the flow rate could not be estimated. The last opportunity was at 23:00 on November 7, 2016, when the flow was not noticeable, either because the flow rate was very low or because the flow of drilling mud out from the well head had stopped. These observations suggest that the flow was transient and lasted for at least 3 days.

One may think that the observed flow could be caused by swabbing force; that reduces the bottom hole pressure below the formation pressure due to the effects of pulling the drill string, which allows an influx of formation fluids into the borehole. However, the swabbing force operates only when the string moves within the borehole, and is dispersed almost immediately after the drill string is pulled out of the borehole. When we observed the upwelling flow using the underwater camera, at least four hours had passed since the string was removed from the borehole. Therefore, the observed flow was solely generated by natural overpressure in the formation.

4.2. Analysis of Transient Upwelling Flow

We employed a simple numerical model to explain the observed transient flow and estimate ΔP (Figure 3a). A disk-shaped, horizontal, overpressured aquifer of finite thickness was assumed as structural components such as décollement and bedding tend to be nearly horizontal (see 2. Geology at Site 0023). The aquifer was set at a depth of 1,000 mbsf to coincide with the interval of the highest excess pore pressure in LSB facies (Figure 2b), and to coincide with a period of loss of torque on the drill bit that likely indicated drilling through an aquifer (Hamada et al., 2018).

The pore pressure distribution in a circular aquifer is given by the radial diffusion equation

$$\frac{\partial^2 \Delta P}{\partial r^2} + \frac{1}{r} \frac{\partial \Delta P}{\partial r} = \frac{\phi \mu \beta}{k} \frac{\partial \Delta P}{\partial t}, \quad (5)$$

where ΔP is excess pore pressure (overpressure), r is the radial distance, k is the permeability, ϕ is the porosity (0.34) which is the measured value from cores around 1,000 mbsf (Figure 2a), μ is the dynamic viscosity of formation fluid (3.0×10^{-4} Pa s at 100°C), and β is the fluid compressibility (4.0×10^{-10} Pa⁻¹). The analytical solution, assuming the aquifer radius (r_{\max}) to be infinite, has been derived in previous studies (e.g., Becker et al., 1983; Fisher et al., 1997; Jaeger & Clark, 1942), where the pore pressure and flow rate of the fluid injected from the aquifer are expressed as

$$p(r, t) = \Delta P + \frac{2\Delta P}{\pi} \int_0^\infty e^{-\tau u^2} \frac{J_0\left(\frac{ur}{a}\right) Y_0(u) - Y_0\left(\frac{ur}{a}\right) J_0(u)}{J_0^2(u) + Y_0^2(u)} \frac{du}{u}, \quad (6)$$

and

$$Q = \pi a^2 v = \frac{2\pi r H k}{\mu} \frac{\partial p}{\partial r}, \quad (7)$$

where $\tau \equiv kt/\phi\mu\beta a^2$, Q is the flow rate (7.8×10^{-3} m³ s⁻¹ on November 1, which is calculated from the measured flow velocity, $v = 0.1$ m s⁻¹ and borehole radius, $a = 0.16$ m), H is the thickness of the aquifer, J_0 and Y_0 are Bessel functions of the first and second kind of orders, and u is variable of integration. Clearly, for an infinite-aquifer model, the flow rate decreases very slowly with time. However, the observed flow became unnoticeable within a few days suggesting a rapid decrease in flow rate and therefore, an aquifer of finite extent. We therefore also solved Equation 5 for a finite aquifer with boundary conditions expressed as

$$\Delta P|_{r \leq a} = 0 \text{ and } \frac{\partial \Delta P}{\partial r} \Big|_{r=r_{\max}} = 0. \quad (8)$$

The flow velocity for this model was also calculated from the pressure gradient as shown in Equation 7. The excess pore pressure ΔP and flow rate Q for finite aquifers with different radial distances ($r_{\max} = \text{infinite, 10, 100, and 1,000 m}$) and thicknesses ($H = 1, 10, \text{ and } 100 \text{ m}$), were also calculated.

4.2.1. Indicative Value of Permeability

To make a first-pass estimate of ΔP and Q for the aquifer, an indicative value of k was needed. If the décollement zones are considered to be representative of aquifers in accretionary wedges, permeability measurements from other décollement zones can provide a range of likely values for our theoretical aquifer.

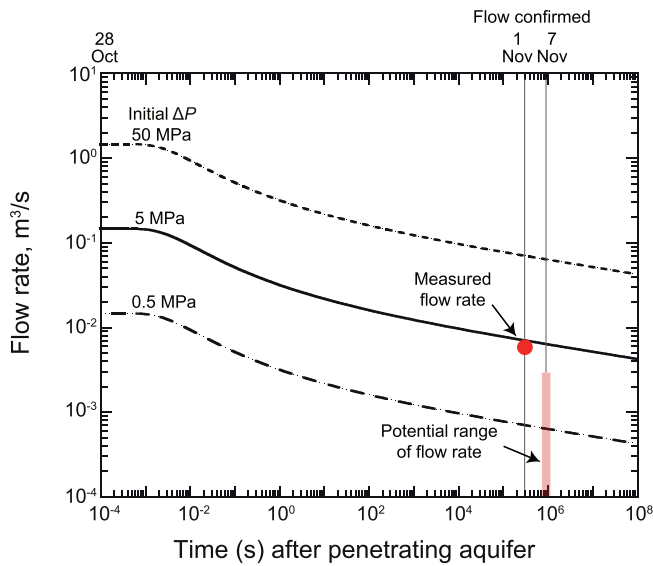


Figure 4. Log-log plot of modeled rate of flow up the borehole versus time after penetration of a theoretical disk-shaped infinite aquifer. Curves are shown for three initial values of ΔP for an infinite aquifer with permeability of 10^{-13} m^2 and thickness of 10 m. Also shown is the measured flow rate on November 1 (solid red dot; estimated from video) and the potential range of flow rates on November 7 (pink vertical bar).

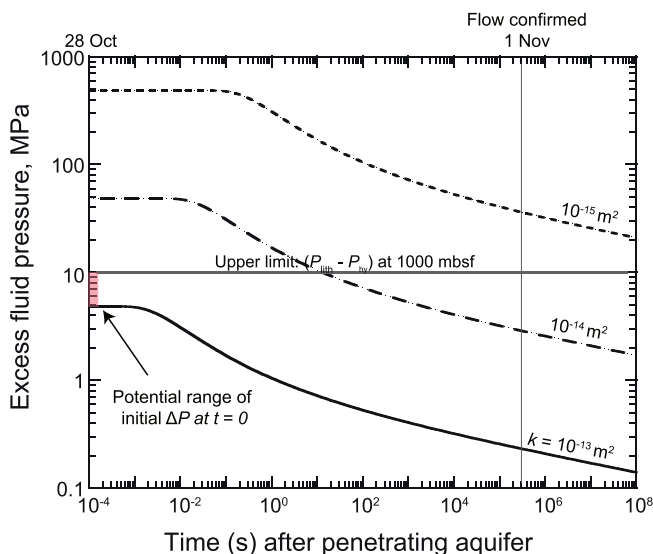


Figure 5. Log-log plot of modeled excess fluid pressure above hydrostatic pressure (ΔP) versus time after penetration, for an infinite aquifer at $r = 2a$. Curves are shown for three different aquifer permeabilities assuming an initial ΔP of 5 MPa and aquifer thickness of 10 m. An initial ΔP of 5 MPa was chosen as it best fits the measured flow rates on November 1 (see Figure 4). The upper limit of ΔP is constrained by the vertical effective stress ($\sim 10 \text{ MPa}$ at 1,000 mbsf at Site C0023).

Bulk permeabilities of 10^{-16} to 10^{-13} m^2 have been determined at the décollement of the Nankai, Costa Rica, and Barbados subduction zones by methods including modeling and laboratory measurements (Bekins et al., 1995; Saffer & Bekins, 1998; Skarbek & Saffer, 2009; Spinelli et al., 2006). These values are similar to (or slightly lower than) those estimated from tests in a borehole in the Barbados décollement zone (10^{-15} to 10^{-13} m^2 ; Fisher et al., 1996). Although permeability changes with effective stress, a value of 10^{-13} m^2 was considered to be a reasonable upper limit for permeability for our aquifer models.

4.2.2. Estimation of Transient Flow Rates

An aquifer permeability $k = 10^{-13} \text{ m}^2$ and thickness $H = 10 \text{ m}$ were first used in Equation 5 and the initial ΔP in the theoretical infinite aquifer was changed, to find a reasonable initial ΔP that can explain the observed flow rate. The thickness of the aquifer was considered to be less than the vertical resolution of the seismic survey data ($\sim 15 \text{ m}$) because no strong seismic reflection characteristics of zones of high pore pressure were visible in LSB facies (Figure 1b). Nine model aquifers of different finite extents were then considered. By modeling these aquifers with different values of r and H , time evolutions of flow rates were obtained, which were then compared with the flow rates observed at the head of the casing pipe at Site C0023.

4.3. Results of Analysis

4.3.1. Infinite Aquifer

Figure 4 shows the results of modeling for the borehole flow rate with time after penetration of the theoretical aquifers, with different initial ΔP values of 0.5, 5, and 50 MPa for the case of $k = 10^{-13} \text{ m}^2$ and $H = 10 \text{ m}$. The measured flow rate for November 1 fits well with the modeled case for initial $\Delta P = 5 \text{ MPa}$ (Figure 4), whereas the model cannot explain the indistinct flow observed on November 7. Although the infinite model cannot reproduce the overall change in flow rate, using initial $\Delta P = 5 \text{ MPa}$, which is necessary for explaining the flow rate on November 1, we calculated the time evolution of ΔP at $r = 2a$ for this aquifer (Figure 5). $\Delta P|_{r=2a}$ for the aquifer dropped rapidly from 5 to 1 MPa in 2 s after penetration, and became approximately 0.2 MPa on November 1. In Figure 5, the time evolution of $\Delta P|_{r=2a}$ for the case of impermeable aquifers with $k = 10^{-14}$ and 10^{-15} m^2 is plotted. The initial ΔP increased with decreasing aquifer permeability to obtain a flow rate value similar to the one observed for $k = 10^{-13} \text{ m}^2$. When ΔP exceeds the vertical effective stress, the formation tends to fracture leading to a drop in fluid pressure. Therefore, the greatest ΔP in this setting is limited by the vertical effective stress of about 10 MPa, which is the difference between the overburden and hydrostatic pressures calculated at 1,000 mbsf at Site C0023. Considering that the upper limit of permeability of the aquifer is 10^{-13} m^2 , the initial ΔP at Site C0023 likely lies in the range of ~ 5 –10 MPa. The estimated lowest value of initial ΔP is nearly consistent with our estimates of pressure from porosity data at Site C0023 (Figure 2b) and with those reported by Screation et al. (2002) for Sites 1174 and 808.

4.3.2. Finite Aquifers

Since the case of an infinite-aquifer cannot explain the rapid drop in flow rate over time, we calculated the time evolution of flow rate Q and pore

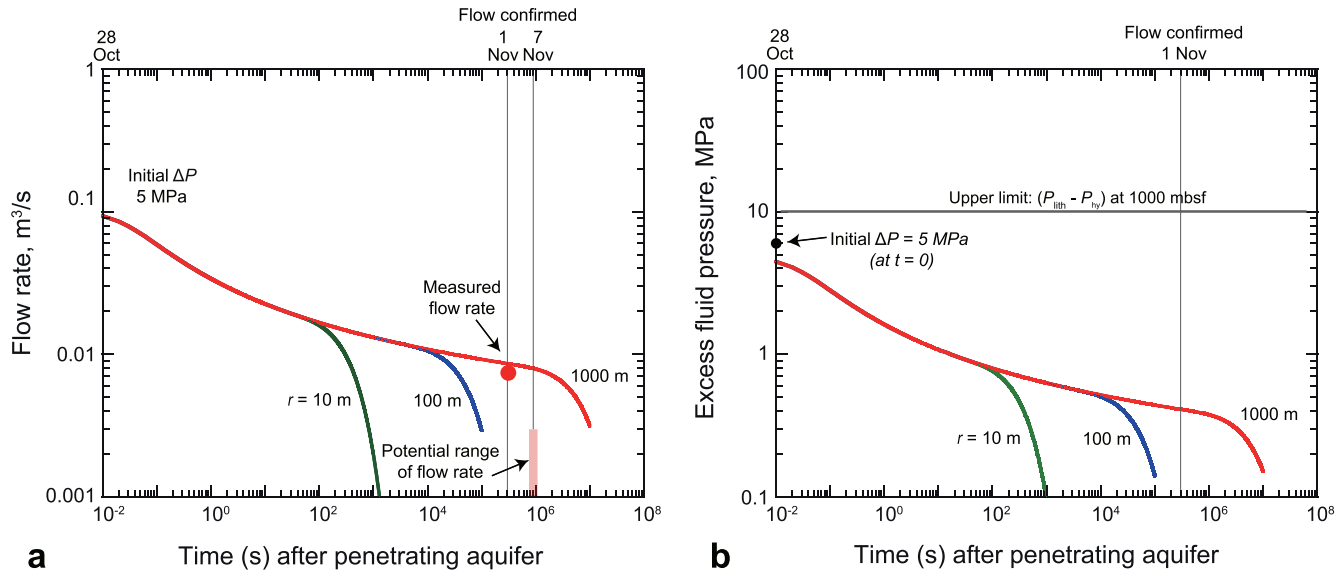


Figure 6. Log-log plots of (a) modeled rate of flow up the borehole (Q) and (b) modeled excess fluid pressure above the hydrostatic pressure (ΔP) at $r = 2a$, versus time after penetration of disk-shaped finite aquifers. Curves are shown for finite aquifers with different radii (r ; green, blue, and red lines), for an initial ΔP of 5 MPa, an aquifer thickness of 10 m and permeability of 10^{-13} m^2 . Also shown in panel (a) is the measured flow rate on November 1 (solid red dot; estimated from video) and the potential range of flow rates on November 7 (pink vertical bar). The upper limit of ΔP is constrained by the by the vertical effective stress ($\sim 10 \text{ MPa}$ at 1,000 mbsf at Site C0023).

pressure ΔP at $r = 2a$ for finite aquifers with different radial distances ($r_{\text{max}} = 10, 100, \text{ and } 1,000 \text{ m}$) (Figure 6). Based on the indicative results for the infinite case, we used thickness $H = 10 \text{ m}$, $k = 10^{-13} \text{ m}^2$, and $\Delta P = 5 \text{ MPa}$ for the model. Figure 6a shows the time evolution of Q . Modeled flow rates decreased earlier as aquifer size decreased. The modeling results indicate that an aquifer with a radius of several hundred meters ($100 \text{ m} \leq r_{\text{max}} \leq 1,000 \text{ m}$) is a necessary condition to explain the observed change in flow rate over time. Considering a time evolution of $\Delta P|_{r=2a}$ for aquifers of finite radial extent (Figure 6b), $\Delta P|_{r=2a}$ for the aquifer with a 10 m radius dropped below 0.1 MPa 10 min after penetration, whereas for the aquifer with a radius of 1,000 m, the drop happened after 100 days.

Figure 7 shows the time evolution of flow rate for aquifers with different thicknesses ($H = 1, 10, \text{ and } 100 \text{ m}$) and radii ($r_{\text{max}} = 10, 100, \text{ and } 1,000 \text{ m}$) for the initial $\Delta P = 5 \text{ MPa}$ and $k = 10^{-13} \text{ m}^2$. The measured flow rate on November 1 fits the modeled case well for $H = 10 \text{ m}$ and $r_{\text{max}} = 1,000 \text{ m}$, or $H = 100 \text{ m}$ and $r_{\text{max}} = 100 \text{ m}$.

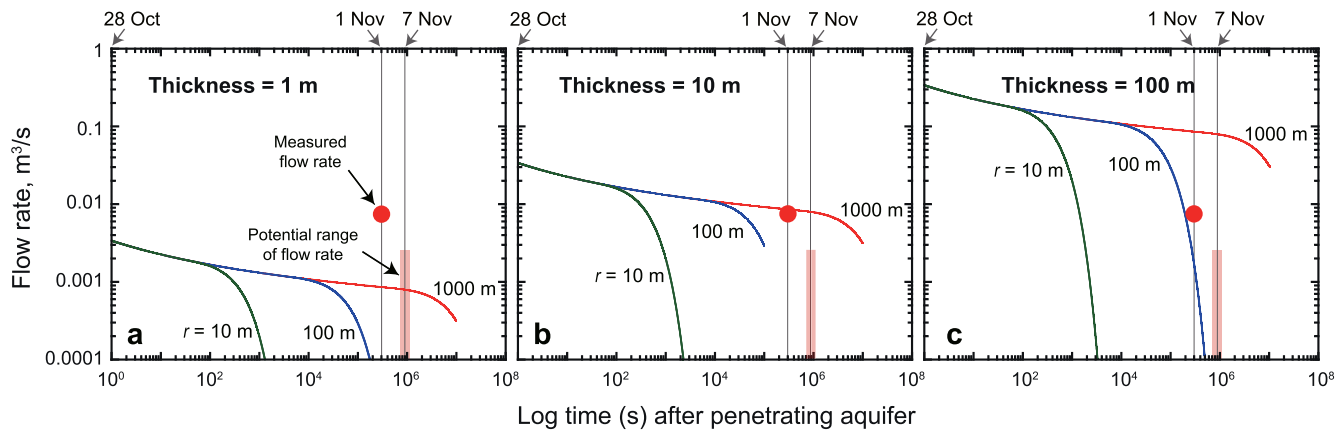


Figure 7. Log-log plot of modeled rate of flow up the borehole versus time after penetration of aquifers with thicknesses of (a) 1 m, (b) 10 m, and (c) 100 m. Curves are shown for three finite aquifers with different radii (r ; green, blue, and red lines) for an initial ΔP of 5 MPa and permeability of 10^{-13} m^2 . Also shown is the measured flow rate on November 1 (solid red dot) and the potential range of flow rates on November 7 (pink vertical bar). Measured flow rates can be best explained by aquifers with sizes ranging from $\sim 3 \times 10^6 \text{ m}^3$ ($H = 100 \text{ m}$ and $r = 100 \text{ m}$ in panel (c)) to $\sim 3 \times 10^7 \text{ m}^3$ ($H = 10$ and $r = 1,000 \text{ m}$ in panel (b)).

(Figure 5b and 5c, respectively). On the other hand, for an aquifer with $H = 1$ m, all modeled flow rates are lower by one order of magnitude compared to the measured flow rate for November 1 (Figure 5a). The modeling results suggest that the observed change in flow rate with time can be explained by an aquifer with a radial distance of several hundred meters and a thickness of tens of meters (i.e., the total volume of the aquifer ranging from $\sim 3 \times 10^6$ to $\sim 3 \times 10^7$ m³).

5. Discussion

5.1. Distribution of Porosity With Depth at Neighboring Sites

Although the overall trends of porosity with depth at Sites C0023, 808, and 1174 are similar (Figures 2 and S1), the depths at which overpressure occurs in the underthrust sediments differ among these neighboring sites. Porosity in the underthrust sediments at Site 808 follows the curve for a ΔP of 4.2 MPa, from 960 mbsf (just below the décollement), whereas at Site 1174 porosity follows the curve corresponding to a ΔP of 3.6 MPa from 900 mbsf (~ 40 m below the décollement) (Screaton et al., 2002). In contrast, the porosity profile at Site C0023 (Figure 2b) shows that ΔP increases gradually from 2 MPa at the base of the décollement zone at 800 mbsf to 4.2 MPa at about 1,020 mbsf, and then decreases to 3 MPa at the base of the underthrust sequence at 1120 mbsf. The overall trend of ΔP suggests that high-pressure fluid has diffused both upward and downward from the aquifer at ~ 1020 mbsf at Site C0023, and that the ranges of ΔP in the underthrust sediments are identical among the three sites. However, the depth distributions of ΔP differ among the three sites, even though they are within 3 km of each other. This in turn may suggest that the high-pressure aquifers at the three sites are likely not connected, and that their lateral extents are smaller than the distances between them, which is implied by the finite aquifer modeling described above.

5.2. Pore Pressure and Size of Aquifer

Porosity changes are only partially reversible in response to a decrease in effective stress with increasing pore pressure, because cohesion of the sediments increases with time and pressure. Therefore, the pore pressures we estimated from porosity data at Site C0023 (Figure 2b) may represent the minimum ΔP that has been generated since the deposition of LSB facies during the Pliocene (Screaton et al., 2002). However, the pressure we estimated from the upwelling flow, which reflects the current state of pore pressure (Figure 5), is slightly higher than the minimum pressure estimated from the porosity data. Although matching the two estimates is not required, the difference between the two likely reflects the uncertainties in the permeability of the modeled aquifer. Consequently, uncertainties remain in our modeled values of ΔP . Nonetheless, the important observation is that the flow from the head of the casing pipe clearly decreased with time, and became unnoticeable five days after it was first observed. Based on this rapid decrease of the flow rate, we infer that drilling at Site C0023 intersected a relatively small, disconnected high-pressure aquifer, possibly of several hundred meters lateral extent and several tens of meters vertical extent (Figures 6 and 7), within the underthrust sediments. Moreover, the differences in the depth profile of porosity-based ΔP among Sites C0023, 808, and 1174 (see 5.1) suggest that the aquifers penetrated by each borehole may have different pressure regimes. Our results therefore suggest that the region of high pore pressure below the décollement at Site C0023 represents one of many sub-kilometer overpressured aquifers that are patchily distributed within the underthrust sediments, each with perhaps different degrees of excess pore pressure.

5.3. Implication for Slow Earthquakes

Various types of slow earthquake including tremors, very low-frequency events, and slow slip events, have been observed in the shallow plate-boundary region along the Nankai Trough (e.g., Obara & Kato, 2016; Yokota et al., 2016). Slow earthquakes have also been reported in the vicinity of the drilling sites we investigated (e.g., Nakano et al., 2018; Takemura et al., 2019; Yokota & Ishikawa, 2020) (Figure 1a). Thus, during Expedition 370 it is likely that the hypocentral area of the slow earthquakes was penetrated as the borehole was drilled through the décollement and into the basaltic basement. Seismic surveys have indicated a possible linkage between the zone of high pore pressure and the distribution of slow earthquakes in the Nankai Trough (e.g., Kodaira et al., 2004). Kitajima and Saffer (2012) estimated pore pressures from the hydromechanical properties of sediment samples from the Nankai accretionary prism, and also showed that

the region of highest pore pressure corresponds to the source area of the slow earthquakes that have been detected. It is thought that an increase in pore pressure reduces the effective normal stress on a fault plane, leading to low shear strength and slow slip. Hence, high pore pressure zones are considered to be potential sites that trigger slow earthquakes.

According to laboratory friction experiments and theoretical analysis of a simple spring-slider model, stable and unstable fault slip depend on the interaction between a critical stiffness of a fault, K_{cr} , defined in Equation 9, and the elastic stiffness of the surrounding country rock, K (Rice & Ruina, 1983)

$$K_{cr} = \frac{-(a-b)\sigma_n^{eff}}{D_c} \quad (9)$$

where σ_n^{eff} is effective normal stress, D_c is critical slip distance and $(a-b)$ is combined friction parameter. When $(a-b)$ is positive, stable slip occurs ($K_{cr} < 0 < K$). When $(a-b)$ is negative, slip is either unstable ($0 < K < K_{cr}$) or conditionally stable ($0 < K_{cr} < K$). The latter case, particularly at $K_{cr} \sim K$, represents the range of conditions thought to be most favorable for generating slow slip (Leeman et al., 2016).

Pore pressure could impact both K_{cr} and K . For example, the results of high-temperature and -pressure friction experiments by Okamoto et al. (2020) suggest that K_{cr} changes with pore fluid pressure and becomes closer to K for a given temperature and pressure condition, which is a mechanical prerequisite for the generation of slow earthquakes. Increasing pore pressure may also reduce the elastic stiffness K as a result of hydraulic fracturing, potentially meeting conditions ($K_{cr} \sim K$) favorable for generating slow earthquakes. However, the effects of pore pressure on both K_{cr} and K remain unclear. Further study is needed to investigate the physical effects of pore pressure change on K_{cr} and K in order to fully understand the generation of slow earthquakes.

Expedition 370 provides the first known penetration of a hypocentral region of shallow slow earthquakes at a subduction zone plate boundary (Figure 1). Although the geophysical survey data do not provide accurate depths for these earthquakes off Cape Muroto, the slow earthquakes there can be attributed not only to slip at the décollement but also to slow slip related to a patchy distribution of overpressured aquifers in the underthrust sediments.

6. Conclusions

We used two methods to analyze drilling data obtained at Site C0023 during IODP Expedition 370 and to estimate pore pressures within underthrust sediments in the Nankai subduction zone off Cape Muroto. First, we examined the trend of porosity with depth from core samples in the Lower Shikoku Basin facies, which includes the décollement zone; the excess pore pressure increased gradually from about 2 MPa at the base of the décollement zone at 800 mbsf to about 4.2 MPa ($\lambda^* = \sim 0.42$) at 1,020 mbsf, and then decreased to ~ 3 MPa ($\lambda^* = \sim 0.3$) just above the basement at 1,120 mbsf. Next, the excess pore pressure was estimated by analyzing the transient upwelling flow of drilling mud from the borehole, that was observed during drilling. This observation provided the first direct evidence of overpressured sediment beneath the décollement off Cape Muroto. A radial diffusion equation was solved to model the initial excess pore pressure and the size of the aquifer, in order to explain the observed flow rate and duration of the upwelling mud flow. It was observed that for a permeability of 10^{-13} m^2 , the aquifer possessed an initial excess pore pressure of more than 5 MPa ($\lambda^* = \sim 0.5$) above the hydrostatic pressure, and that its size extended several hundred meters laterally and several tens of meters in thickness.

Our results combined with the depth profiles of porosity data at neighboring drill sites suggest that there is a patchy distribution of sub-kilometer aquifers with different degrees of overpressure within the underthrust sediments of the Nankai subduction zone. The presence of these overpressured aquifers may have contributed to the generation of slow earthquakes off Cape Muroto.

Data Availability Statement

The porosity data (moisture and density data) used in Figure 2 and the movie file used in Figure 3b are available online at <http://sio7.jamstec.go.jp/j-cores.data/370/C0023A/> and <http://dx.doi.org/10.17632/mf3rdzt-s4y.1>, respectively.

Acknowledgments

This research used samples and data provided by the International Ocean Discovery Program (IODP). The authors thank the ship's crew, technicians, and scientific party aboard D/V *Chikyu* during Expedition 370. The authors also special thanks to Y. Nanba for the underwater TV operations and D. Saffer, J.D. Bedford and K. Okazaki for their helpful discussions. We are also grateful to reviewers M. Collignon and K. Kanagawa and anonymous associate editor for their constructive comments that helped to improve this manuscript. This work was partly supported by the Japan Society for the Promotion of Science KAKENHI Grant Numbers JP19H02006, JP19K21907, 17H06455, and JP16H06476, by the Scientific Research on Innovative Areas "Science of Slow Earthquakes", and by the Deutsche Forschungsgemeinschaft (DFG, German Research Foundation) under Germany's Excellence Strategy – EXC-2077 – 390741603.

References

- Asano, Y., Obara, K., & Ito, Y. (2008). Spatiotemporal distribution of very-low frequency earthquakes in Tokachi-oki near the junction of the Kuril and Japan trenches revealed by using array signal processing. *Earth, Planets and Space*, 60(8), 871–875. <https://doi.org/10.1186/BF03352839>
- Becker, K., Langseth, M. G., & Von Herzen, R. P. (1983). Deep crustal geothermal measurements, Hole 504B, Deep Sea Drilling Project Legs 69 and 70. In Cann, J. R., et al. (Eds.), *Initial Reports DSDP*, 69 (pp. 223–235). Washington DC: US Government Printing Office. <https://doi.org/10.2973/dsdp.proc.69.105.1983>
- Bekins, B. A., McCaffrey, A. M., & Dreiss, S. J. (1995). Episodic and constant flow models for the origin of low-chloride waters in a modern accretionary complex. *Water Resources Research*, 31, 3205–3215. <https://doi.org/10.1029/95WR02569>
- Blum, P. (1997). *Physical properties handbook—A guide to the shipboard measurement of physical properties of deep-sea cores* (Technical Note 26). Ocean Drilling Program. <https://doi.org/10.2973/odp.tn.26.1997>
- Davis, D., Suppe, J., & Dahlen, F. A. (1983). Mechanics of fold-and-thrust belts and accretionary wedges. *Journal of Geophysical Research*, 88, 1153–1172. <https://doi.org/10.1029/JB088iB02p01153>
- Fisher, A. T., Becker, K., & Davis, E. E. (1997). The permeability of young oceanic crust east of Juan de Fuca Ridge determined using borehole thermal measurements. *Geophysical Research Letters*, 24(11), 1311–1314. <https://doi.org/10.1029/97GL01286>
- Fisher, A. T., & Zwart, G. (1996). Relation between permeability and effective stress along a plate-boundary fault, Barbados accretionary complex. *Geology*, 24, 307–310. [https://doi.org/10.1130/0091-7613\(1996\)024<0307:RBPAAES>2.3.CO;2](https://doi.org/10.1130/0091-7613(1996)024<0307:RBPAAES>2.3.CO;2)
- Gamage, K., & Scream, E. (2006). Characterization of excess pore pressures at the toe of the Nankai accretionary complex, Ocean Drilling Program sites 1173, 1174, and 808: Results of one-dimensional modeling. *Journal of Geophysical Research*, 111, B04103. <https://doi.org/10.1029/2004JB003572>
- Hamada, Y., Hirose, T., Ijiri, A., Yamada, Y., Sanada, Y., Saito, S., et al. (2018). In-situ mechanical weakness of subducting sediments beneath a plate boundary décollement in the Nankai Trough. *Progress in Earth and Planetary Science*, 5, 70. <https://doi.org/10.1186/s40645-018-0228-z>
- Heuer, V. B., Inagaki, F., Morono, Y., Kubo, Y., Maeda, L., et al. (2017). Temperature limit of the deep bio-sphere off Muroto. In *Proceedings of the International Ocean Discovery Program*, 370. College Station, TX: International Ocean Discovery Program. <https://doi.org/10.14379/iodp.proc.370.103.2017>
- Jaeger, J. C., & Clark, M. (1942). A short table of I(O, I; x). In *Proceedings of the royal society of Edinburg*, A (Vol. 61, pp. 229–230).
- Kitajima, H., & Saffer, D. M. (2012). Elevated pore pressure and anomalously low stress in regions of low frequency earthquakes along the Nankai Trough subduction megathrust. *Geophysical Research Letters*, 39, L23301. <https://doi.org/10.1029/2012GL053793>
- Kodaira, S., Iidaka, T., Kato, A., Park, J. O., Iwasaki, T., & Kaneda, Y. (2004). High pore fluid pressure may cause silent slip in the Nankai Trough. *Science*, 304(5676), 1295–1298. <https://doi.org/10.1126/science.1096535>
- Leeman, J. R., Saffer, D. M., Scuderi, M. M., & Marone, C. (2016). Laboratory observations of slow earthquakes and the spectrum of tectonic fault slip modes. *Nature Communications*, 7, 11104. <https://doi.org/10.1038/ncomms11104>
- Moore, G. F., Taira, A., Klaus, A., & Becker, A. (2001). *Proceedings of the Ocean drilling Program* Initial Reports 190. College Station, TX: Ocean Drilling Program. <https://doi.org/10.2973/odp.proc.ir.190.2001>
- Moore, J. C., & Vrolijk, P. (1992). Fluids in accretionary prisms. *Reviews of Geophysics*, 30, 113–135. <https://doi.org/10.1029/92RG00201>
- Nakano, M., Hori, T., Araki, E., Kodaira, S., & Ide, S. (2018). Shallow very-low-frequency earthquakes accompany slow slip events in the Nankai subduction zone. *Nature Communications*, 9(1), 984. <https://doi.org/10.1038/s41467-018-03431-5>
- Obara, K., & Kato, A. (2016). Connecting slow earthquakes to huge earthquakes. *Science*, 353(6296), 253–257. <https://doi.org/10.1126/science.aaf1512>
- Okamoto, A., Niemeijer, A. R., Takeshita, T., Verberne, B. A., & Spiers, C. J. (2020). Frictional properties of actinolite-chlorite gouge at hydrothermal conditions. *Tectonophysics*, 779, 228377. <https://doi.org/10.1016/j.tecto.2020.228377>
- Rice, J. R., & Ruina, A. L. (1983). Stability of steady frictional slipping. *Journal of Applied Mechanics*, 50(2), 343–349. <https://doi.org/10.1115/1.3167042>
- Rubey, W. W., & Hubbert, M. K. (1959). Role of fluid pressure in mechanics of overthrust faulting. II. Overthrust belt in geosynclinal area of western Wyoming in light of fluid-pressure hypothesis. *Geological Society of America Bulletin*, 70, 167–205. [https://doi.org/10.1130/0016-7606\(1959\)70\[167:rofpm\]2.0.co;2](https://doi.org/10.1130/0016-7606(1959)70[167:rofpm]2.0.co;2)
- Saffer, D. M. (2003). Pore pressure development and progressive dewatering in underthrust sediments at the Costa Rican subduction margin: Comparison with northern Barbados and Nankai. *Journal of Geophysical Research*, 108(B5), 2261. <https://doi.org/10.1029/2002JB001787>
- Saffer, D. M., & Bekins, B. A. (1998). Episodic fluid flow in the Nankai accretionary complex: Timescale, geochemistry, and fluid budget. *Journal of Geophysical Research*, 103, 30351–30370. <https://doi.org/10.1029/98JB01983>
- Saffer, D. M., & Tobin, H. J. (2011). Hydrogeology and mechanics of subduction zone forearcs: Fluid flow and pore pressure. *Annual Review of Earth and Planetary Sciences*, 39, 157–186. <https://doi.org/10.1146/annurev-earth-040610-133408>
- Scholz, C. H. (1998). Earthquakes and friction laws. *Nature*, 391, 37–42. <https://doi.org/10.1038/34097>
- Scream, E. J., Saffer, D. M., Henry, P., & Hunze, S. (2002). Porosity loss within the underthrust sediments of the Nankai accretionary complex: Implications for overpressures. *Geology*, 30(1), 19–22. [https://doi.org/10.1130/0091-7613\(2002\)030<0019:PLWTUS>2.0.CO;2](https://doi.org/10.1130/0091-7613(2002)030<0019:PLWTUS>2.0.CO;2)
- Shipboard Scientific Party. (1991). Site 808. In Taira, A., Hill, I., Firth, J. V., et al. (Eds.), *Proceedings of the ocean drilling program*, Initial Reports 131 (pp. 71–269). College Station, TX: Ocean Drilling Program. <https://doi.org/10.2973/odp.proc.ir.131.106.1991>
- Shipboard Scientific Party. (2001a). Site 1173. In Moore, G. F., Taira, A., Klaus, A., et al. (Eds.), *Proceedings of ocean drilling program*, Initial Reports 190 (pp. 1–147). College Station, TX: Ocean Drilling Program. <https://doi.org/10.2973/odp.proc.ir.190.104.2001>
- Shipboard Scientific Party. (2001b). Site 1174. In Moore, G., Taira, A., Klaus, A., et al. (Eds.), *Proceedings of ocean drilling program*, Initial Reports 190 (pp. 1–149). College Station, TX: Ocean Drilling Program. <https://doi.org/10.2973/odp.proc.ir.190.105.2001>

- Shi, Y., & Wang, C. Y. (1988). Generation of high pore pressures in accretionary prisms: Inferences from the Barbados Subduction Complex. *Journal of Geophysical Research*, 93(B8), 8893–8910. <https://doi.org/10.1029/JB093iB08p08893>
- Skarbek, R. M., & Saffer, D. M. (2009). Pore pressure development beneath the décollement at the Nankai subduction zone: Implications for plate boundary fault strength and sediment dewatering. *Journal of Geophysical Research*, 114, B07401. <https://doi.org/10.1029/2008JB006205>
- Spinelli, G. A., Saffer, D. M., & Underwood, M. B. (2006). Hydrogeologic responses to three-dimensional temperature variability, Costa Rica subduction margin. *Journal of Geophysical Research*, 111, B04403. <https://doi.org/10.1029/2004JB003436>
- Takemura, S., Matsuzawa, T., Noda, A., Tonegawa, T., Asano, Y., Kimura, T., & Shiomi, K. (2019). Structural characteristics of the Nankai Trough shallow plate boundary inferred from shallow very low frequency earthquakes. *Geophysical Research Letters*, 46, 4192–4201. <https://doi.org/10.1029/2019GL082448>
- Tobin, H. J., & Kinoshita, M. (2006). *Investigations of seismogenesis at the Nankai Trough, Japan*. (NanTroSEIZE Stage). Integrated Ocean Drilling Program Scientific Prospectus. <https://doi.org/10.2204/iodp.sp.nantroseize1.2006>
- Tobin, H. J., & Saffer, D. M. (2009). Elevated fluid pressure and extreme mechanical weakness of a plate boundary thrust, Nankai Trough subduction zone. *Geology*, 37(8), 679–682. <https://doi.org/10.1130/G25752A.1>
- Tsuji, T., Tokuyama, H., Costa Pisani, P., & Moore, G. (2008). Effective stress and pore pressure in the Nankai accretionary prism off the Muroto Peninsula, southwestern Japan. *Journal of Geophysical Research*, 113, B11401. <https://doi.org/10.1029/2007JB005002>
- Yokota, Y., & Ishikawa, T. (2020). Shallow slow slip events along the Nankai Trough detected by GNSS-A. *Science Advances*, 6, eaay5786. <https://doi.org/10.1126/sciadv.aay5786>
- Yokota, Y., Ishikawa, T., Watanabe, S., Tashiro, T., & Asada, A. (2016). Seafloor geodetic constraints on interplate coupling of the Nankai Trough megathrust zone. *Nature*, 534, 374–377. <https://doi.org/10.1038/nature17632>